LAWRENCE
LIVERMORE
NATIONAL
LABORATORY

LLNL-CONF-698884

Hotspot Electron Temperature from X-Ray Continuum Measurements on the NIF

L. C. Jarrott, L. R. Benedetti, H. Chen, N. Izumi, S. F. Khan, T. Ma, S. R. Nagel, O. L. Landen, A. Pak, P. K. Patel, M. Schneider, H. A. Scott

July 29, 2016

High Temperature Plasma Diagnostics
Madison, WI, United States
June 5, 2016 through June 9, 2016

Disclaimer

Hotspot electron temperature from x-ray continuum measurements on the NIF[a)]

L.C. Jarrott,[1, b)] L.R. Benedetti,[1] H. Chen,[1] N. Izumi,[1] S.F. Khan,[1] T. Ma,[1] S.R. Nagel,[1] O.L. Landen,[1] A. Pak,[1] P.K. Patel,[1] M. Schneider,[1] and H.A. Scott[1]
Lawrence Livermore National Laboratory, Livermore, California 94550, USA

(Dated: 21 July 2016)

We report on measurements of the electron temperature in the hotspot of inertially confined, layered, spherical implosions on the National Ignition Facility using a differential filtering diagnostic. Measurements of the DT and DD ion temperatures using neutron time-of-flight detectors are complicated by the contribution of hot spot motion to the peak width, which produce an apparent temperature higher than the thermal temperature. The electron temperature is not sensitive to this non-thermal velocity and is thus a valuable input to interpreting the stagnated hot spot conditions. Here we show that the current differential filtering diagnostic provides insufficient temperature resolution for the hot spot temperatures of interest. We then propose a new differential filter configuration utilizing larger pinhole size to increase spectral fluence, as well as thicker filtration. This new configuration will improve measurement uncertainty by more than a factor of three, allowing for a more accurate hotspot temperature.

I. INTRODUCTION

At the National Ignition Facility (NIF), indirectly driven, inertial confinement fusion (ICF) experiments[1–3] compress a spherical capsule comprised of deuterium and tritium by using x-ray driven ablation pressure on the capsule. In these experiments, a spherical plastic "ablator" roughly 200 µm thick and 2.2 mm in diameter is filled with deuterium and tritium which is then cryogenically frozen producing an ice layer 70 µm thick on the inner surface of the plastic ablator with a total mass of roughly 170 µg. Inside the frozen DT ice layer is 1 µg of gaseous DT. As the capsule implodes, the kinetic energy of the imploding capsule is converted into internal energy in the DT gas (hotspot) within the shell. As the temperature of the hotspot increases, the deuterium and tritium begin to fuse, producing 14.1 MeV neutrons and 3.5 MeV alpha-particles. For ignition to occur, the hotspot must reach temperatures > 4 keV, with a hotspot areal density on the order of an alpha-particle stopping range, $\sim 0.3 \mathrm{g/cm^2}$, allowing for the alpha-particles to deposit their energy locally, providing additional heating which initiates a fusion bootstrap effect in the hotspot which then causes a fusion burnwave to propagate through the DT ice layer or "fuel".

With temperatures on the order of 4 keV within the hotspot, a significant amount of x-rays are produced in the form of bremsstrahlung radiation. Functionally, this emission takes the form of an exponential distribution of photons which can be parameterized by the local temperature of the emitting region. The temperature of the hotspot plasma can then be characterized in time and space by measuring this emission. This type of measurement has been done previously on the NIF, the design of which has been well described in previous work[4,5]. In this previous work, differential filters in a Ross[6] configuration were used to acquire broadband x-ray signal from the hotspot which was then analyzed to infer an electron temperature of the hotspot. With improvements to the overall performance of ICF implosions on the NIF, the hotspot temperature and overall x-ray fluence has increased bringing about a need for a filter configuration better suited for temperatures currently achieved. Here we present a differential filter setup coupled with variable pinhole diameter sizes to optimize the measurement of higher temperature plasmas.

II. THE DIFFERENTIAL FILTER SPECTROMETER

A. Design

The Titanium Differential Filter Spectrometer (TiDFS) is a time-integrated x-ray pinhole camera situated on the Polar DIM of the NIF. It consists of a pinhole array which it shares with the NIF Gated X-ray Detector (GXD), located 100 mm from target chamber center, with pinhole diameters of both 10 µm and 50 µm. The pinhole substrate is 75 µm thick tantalum. An illustration of the pinhole layout can be seen in figure 1a. The filtering for the TiDFS consists of six titanium filters with thicknesses of 10 µm, 22 µm, 70 µm, 250 µm, 550 µm and 920 µm. The thickest three filters utilize the larger, 50 µm diameter pinholes to maintain good signal to noise. The specific choice of filter thickness and pinhole diameter are discussed in section IV. The filters are situated in an aluminum frame positioned directly in front of, and surrounding the micro-channel plate of the GXD. The distance from the pinhole array to the filter/film assembly is 1118 mm resulting in an image magnification of ~ 11. The recording medium used is

[a)] Contributed paper published as part of the Proceedings of the 21st Topical Conference on High-Temperature Plasma Diagnostics, Madison, Wisconsin, June, 2016.
[b)] Author to whom correspondence should be addressed: jarrott1@llnl.gov

the Fuji SR-type image plate (IP) detector. Imaging plates[7] are sensitive over a wide x-ray energy range, provide reasonable spatial resolution, are robust against electromagnetic pulses (EMP) and high neutron yield (up to ∼mid 10^{15}), and are much simpler to process than traditional emulsion films.

B. Filter Characterization

To characterize the filter thicknesses, the transmission of each filter was measured using an x-ray source. For each filter, a range of x-ray energies were chosen to fit within a transmission range of 5-80% for the given nominal filter thickness. The transmission was calculated by comparing the total fluence from the x-ray source with and without the filter in place. The results of this calibration can be seen in fig. 1, with the error bars representing one standard deviation in the measurement error. Each filter used a minimum of five x-ray energy bands, the results of which were fit to a titanium transmission curve with the filter thickness being calculated by finding a minimum regression of the tabulated data and the transmission curve.

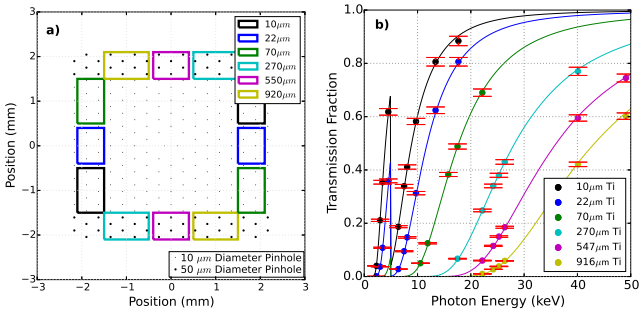

FIG. 1. (a) Pinhole array design utilizing both 10 µm (left and right) and 50 µm (top and bottom) diameter pinholes. (b) Filter thickness characterization using an x-ray source with several line energies for each filter. Error bars correspond to one sigma variance in measurement.

Additionally, the filters were measured using a Heidenhain thickness gauge (model ND-280). Each filter was measured at a single position close to the center of the filter. The results of these measurements show general agreement with the transmission measurements to within 5%. Because impurities within the filters can alter the overall transparency of the filter, the filter thicknesses inferred from the x-ray transmission measurement results are used in the following analysis because they provide a more heuristic measurement for the purposes of this diagnostic.

III. RETROGRADE ANALYSIS OF DATA

With the new filter configuration being comprised entirely of titanium, a Ross analysis could no longer be done. Rather, a retrograde analysis is done where a synthetic x-ray spectrum is folded into the response of each filter as well as the image plate detector response, resulting in a synthetic signal for each filter in units of photo-stimulated luminescence (PSL)[7], identical to the empirical data. The synthetic signals for each filter is then fit to the real data using a linear regression, where a reduced χ^2 fit is calculated for a given temperature and shell attenuation. This process is repeated, scanning through temperature and shell attenuation parameter space until a minimum reduced χ^2 is found.

The equation for the x-ray spectrum can be seen in eq. 1 and is constructed using Kirchoffs law and a fit to the DCA[8] opacity tables.

$$H_{e,\nu} \sim \frac{\rho^2}{(h\nu)^{0.39} T_e^{0.15}} e^{-h\nu/T_e} e^{-\tau} \tag{1}$$

Where T_e is the parameterized electron temperature and τ is the optical depth of the fuel and the remaining plastic ablator.

IV. FILTER OPTIMIZATION

The basic idea behind improving the temperature measurement was to shift the mean sensitivity of the filters to higher photon energies so as to reduce the amount of shell attenuation that could skew the temperature interpretation. The issue here is that shifting the mean sensitivity requires increasing the filter thickness which in turn reduces the signal to noise. To remedy this, the pinhole diameters were increased from 10 µm to 50 µm for the thickest filters. This is a sacrifice in the spatial resolution in favor of a better temperature measurement. But, keeping some thinner filters with 10 µm pinholes made certain that a spatial analysis of the hotspot could still be made.

The filters were chosen to optimize the electron temperature measurement of the hotspot at the relatively higher, ∼5 keV, temperatures which are currently being reported on the NIF[1]. The normalized filter sensitivity for each filter at 5 keV with an optical depth of $\tau = 0.5$ can be seen in fig. 3. To determine the ideal set of filters, we started with a simplified filter configuration consisting of just two filters. This two-filter configuration was then optimized within three parameter spaces, the spectral separation between the mean response of the filters, the amount of shell attenuation, and the signal-to-noise ratio. To do this, synthetic data was used for two titanium filters ranging 50 µm to 1500 µm in thickness. The previously discussed retrograde analysis was then carried out in a brute-force approach where the synthetic signal

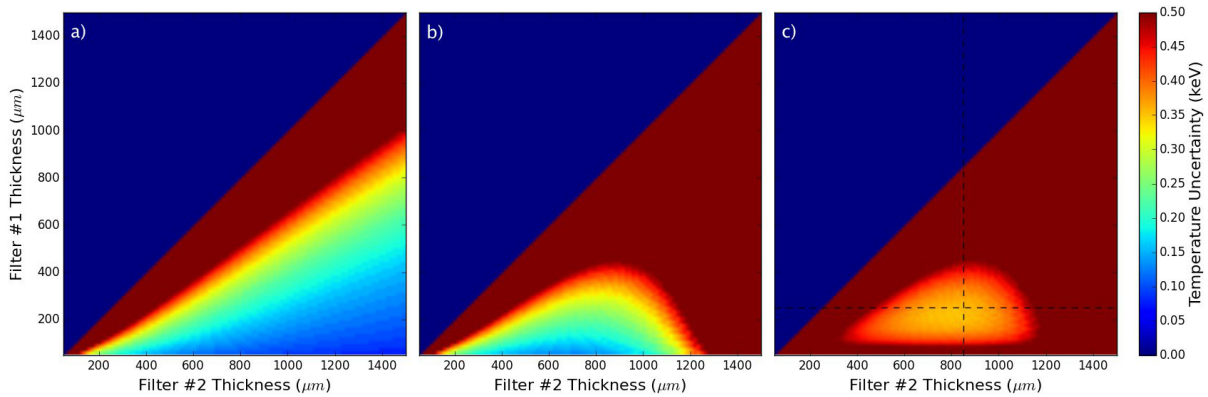

FIG. 2. Two-filter optimization for plasmas > 4 keV. (a) Temperature measurement uncertainty as a function of filter thickness for each filter (#1 and #2) neglecting shell attenuation effects and signal-to-noise. (b) Temperature measurement uncertainty with signal-to-noise factored in. (c) Temperature measurement uncertainty with shell attenuation factored in resulting in an optimized two-filter configuration.

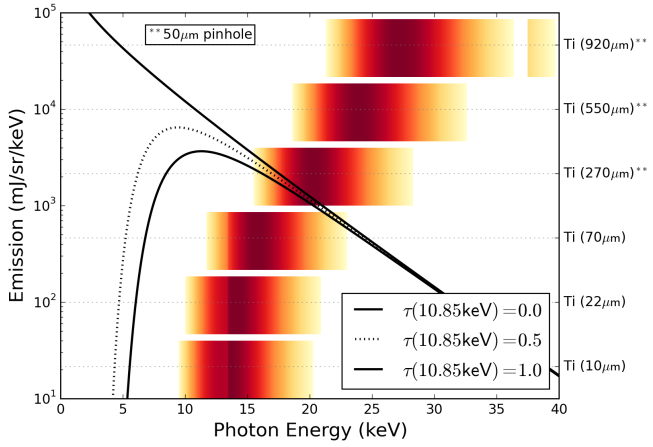

FIG. 3. Normalized filter sensitivity of each filter assuming a 5 keV spectrum with an optical depth at 10.85 keV of 0.5. The optimized, two-filter configuration of 270 µm and 920 µm are shown to have a mean sensitivity significantly outside of the spectral region most sensitive to shell attenuation. Additional filters were added to improve the overall measurement precision.

was allowed to vary randomly by as much as 10%. The choice of 10% came from the nominal empirical variance of the previous Ross filter diagnostic. Once a statistically significant number of iterations had been completed, a variance in the temperature measurement could be calculated. The results of this analysis for all filter thickness and all three parameter scans has been plotted in fig. 2.

Fig. 2 shows the results of the two-filter optimization. Here, in fig. 2a, we see that the temperature measurement is optimized when the thickness of the thinner filter ($f1$) is minimized while the thickness of the thicker filter ($f2$) is maximized. In fig. 2b, signal-to-noise has been factored in. Here we see that $f1$ is still optimized as its thickness is minimized, but $f2$ is now no longer optimized using the thickest possible filtration. There is now a critical thickness for $f2$ where its mean spectral separation balances its signal-to-noise. Now, in fig. 2c, we have included the uncertainty associated with an optical depth ranging from zero to one, evaluated at $h\nu = 10.85$ keV. With this, $f1$ is no longer optimized as its filter thickness goes to zero. Instead, there is an optimum filter thickness that is balanced maximizing the spectral separation between the two filters while simultaneously maximizing the thickness of $f1$ such that the recorded x-ray signal is not dominated by shell attenuation.

This diagnostic is starting to be fielded on high-yield DT implosions. Extraction of hot spot electron temperatures and their comparison to DD and DT ion temperatures will be discussed in a subsequent publication.

ACKNOWLEDGMENTS

This work was performed under the auspices of U.S. Department of Energy by Lawrence Livermore National Laboratory under Contract DE-AC52-07NA27344.

[1]O. Hurricane *et al.*, *Physics of Plasmas (1994-present)*, vol. 21, no. 5, p. 056314, 2014.
[2]M. Edwards *et al.*, *Physics of Plasmas (1994-present)*, vol. 20, no. 7, p. 070501, 2013.
[3]M.J. Edwards *et al.*, *Physics of Plasmas*, vol. 18, no. 5, p. 05100323, 2011.
[4]T. Ma *et al.*, *Review of Scientific Instruments*, vol. 83, no. 10, p. 10E115, 2012.
[5]N. Izumi *et al.*, *Review of Scientific Instruments*, vol. 83, no. 10, p. 10E121, 2012.
[6]P. Ross, *Phys. Rev*, vol. 28, p. 425, 1926.
[7]B. Maddox *et al.*, *Review of Scientific Instruments*, vol. 82, no. 2, p. 023111, 2011.
[8]H. Scott and S. Hansen, *High Energy Density Physics*, vol. 6, no. 1, pp. 39–47, 2010.